Journal of Pharmaceutical Analysis 13 (2023) 673–682

Contents lists available at ScienceDirect

Journal of Pharmaceutical Analysis

journal homepage: www.elsevier.com/locate/jpa

Original article

Tumor cell membrane-coated continuous electrochemical sensor for GLUT1 inhibitor screening

Jiaqian Zhao [a, b], Yuqiao Liu [a], Ling Zhu [a], Junmin Li [a], Yanhui Liu [a], Jiarui Luo [a], Tian Xie [a, b, *], Dajing Chen [a, **]

[a] School of Pharmacy, Hangzhou Normal University, Hangzhou, 310000, China
[b] Innovation Research Institute of Traditional Chinese Medicine, Shanghai University of Traditional Chinese Medicine, Shanghai, 201203, China

ARTICLE INFO

Article history:
Received 13 December 2022
Received in revised form
19 April 2023
Accepted 22 April 2023
Available online 26 April 2023

Keywords:
Glucose transporter 1 inhibitor
Electrochemical sensor
Drug screen
Traditional Chinese medicine

ABSTRACT

Glucose transporter 1 (GLUT1) overexpression in tumor cells is a potential target for drug therapy, but few studies have reported screening GLUT1 inhibitors from natural or synthetic compounds. With current analysis techniques, it is difficult to accurately monitor the GLUT1 inhibitory effect of drug molecules in real-time. We developed a cell membrane-based glucose sensor (CMGS) that integrated a hydrogel electrode with tumor cell membranes to monitor GLUT1 transmembrane transport and screen for GLUT1 inhibitors in traditional Chinese medicines (TCMs). CMGS is compatible with cell membranes of various origins, including different types of tumors and cell lines with GLUT1 expression knocked down by small interfering RNA or small molecules. Based on CMGS continuous monitoring technique, we investigated the glucose transport kinetics of cell membranes with varying levels of GLUT1 expression. We used CMGS to determine the GLUT1-inhibitory effects of drug monomers with similar structures from *Scutellaria baicalensis* and catechins families. Results were consistent with those of the cellular glucose uptake test and molecular-docking simulation. CMGS could accurately screen drug molecules in TCMs that inhibit GLUT1, providing a new strategy for studying transmembrane protein-receptor interactions.
© 2023 The Author(s). Published by Elsevier B.V. on behalf of Xi'an Jiaotong University. This is an open access article under the CC BY-NC-ND license (http://creativecommons.org/licenses/by-nc-nd/4.0/).

1. Introduction

Glucose transporters (GLUTs) are essential membrane proteins in cells that transport glucose via facilitated diffusion to regulate cellular metabolism [1–3]. Tumor cells overexpress GLUTs, particularly glucose transport 1 (GLUT1), to take up enormous amounts of glucose to support their abnormal proliferation, transformation and metastasis [4,5]. GLUT1 is therefore essential for tumor cell proliferation, differentiation, metastasis and prognosis [6–8]. As a result, inhibiting GLUT1 to regulate glucose metabolism is an emerging anti-tumor approach. Some antibodies and small molecules, including BAY-876 [9], epigallocatechin gallate (EGCG) [10], fasentin [11], and phloretin [12], have shown anti-tumor activity by selectively inhibiting GLUT1. However, many of the GLUT1 inhibitor candidates, especially those in traditional Chinese medicines (TCMs), vary significantly in their inhibitory effects despite their similar structures. Effectively screening and analyzing these potential GLUT1 inhibitors therefore remains a challenge in anti-tumor drug discovery.

Current research approaches to GLUT1 are similar to those taken to other membrane proteins, including cryo-scanning electron microscopy, X-ray crystallography, Western blotting, and fluorescent labeling. These analytical methods can measure GLUT1 expression level and characterize GLUT1 structure at the molecular level, but they cannot directly evaluate the transmembrane transport function, which is a key issue in screening GLUT1 inhibitors [13]. It is now possible to extract cell membranes and preserve their biological function in-vitro, offering a platform for studying specific target receptors on the cell membrane [14–16]. With the development of long-term enzyme immobilization, electrochemical glucose sensors can convert concentration changes in glucose into electrical signals, enabling real-time monitoring of molecular transport [17–19]. Therefore, cell membrane-bound electrochemical detection can provide a new method for studying transmembrane protein transport and screening inhibitors targeting GLUT1 [20,21].

Peer review under responsibility of Xi'an Jiaotong University.
* Corresponding author. School of Pharmacy, Hangzhou Normal University, Hangzhou, 310000, China.
** Corresponding author.
E-mail addresses: xbs@hznu.edu.cn (T. Xie), djchen@hznu.edu.cn (D. Chen).

https://doi.org/10.1016/j.jpha.2023.04.015
2095-1779/© 2023 The Author(s). Published by Elsevier B.V. on behalf of Xi'an Jiaotong University. This is an open access article under the CC BY-NC-ND license (http://creativecommons.org/licenses/by-nc-nd/4.0/).

In our previous work, we developed an electrochemical sensor to monitor the transportation kinetics of GLUT1 [22]. In order to better understand the drug inhibitory effect on GLUT1 transport, in this study, we created a tumor cell membrane-based glucose sensor (CMGS) with high sensitivity for GLUT1 inhibitors in TCMs. Enzyme-loaded hydrogel electrodes demonstrated long-term operational stability for continuous electrochemical monitoring. The biocompatible surface of the hydrogel layer can bind to membranes of different cellular origins, including normal cells, tumor cells, and GLUT1 knockdown cells. We investigated the effect of different direct inhibitors and indirect expression regulators. Finally, we employed the CMGS to identify effective GLUT1-inhibitory components in the *Scutellaria baicalensis* and catechins families by screening their derivatives. Screening results were consistent with those of the cellular glucose uptake test and molecular-docking simulation, suggesting that the CMGS could accurately monitor the drug-inhibited GLUT1 transport process under various pharmacological conditions. The reliable screening platform discussed in this paper provides a new strategy for studying transmembrane transporters and developing anti-tumor TCMs.

2. Materials and methods

2.1. Instruments and materials

Cell membranes were extracted by ultra-high speed centrifuge (Beckman MAX-XP, Brea, CA, USA). The surface topologies of electrode were characterized by scanning electron microscopy (SEM, Hitachi SU-8000 field-emission, Tokyo, Japan) and atomic force microscopy (AFM, E-Sweep NanoNavi, Tokyo, Japan). Fluorescent recovery after photobleaching (FRAP) test was performed using laser confocal microscopy (FV 3000, Olympus, Tokyo, Japan). The amperometric response (I-t) were recorded using CHI1000c electrochemical workstation (CH Instruments, Inc., Shanghai, China). Quantitative reverse transcription polymerase chain reaction (RT-qPCR) was tested by Applied Biosystems QuantStudio (Thermo Scientific, Waltham, MA, USA). Glucose uptake of cells was analyzed by microplate reader (Thermo Scientific).

All reagents used in this study are listed in the Supplementary data.

2.2. Preparation of cell membrane vesicles and L-α-phosphatidylcholine vesicles

We prepared cell membrane vesicles using freeze-thaw cycles and gradient centrifugation, with slight modifications from our previous work, and experimental details of small interfering RNA (siRNA) transfection and FRAP can be found in the Supplementary data [22]. All types of tumor cells were resuspended a low osmotic pressure solution (20 mM Tris-HCl, 10 mM KCl, and 2 mM $MgCl_2$) in 4 °C for 48 h to adjust the osmotic pressure. Then the cell suspensions were alternately subjected to ambient temperature and −80 °C temperature for 5 times. The resulting mixture was centrifuged at 20,000 *g* for 30 min, after which the supernatant was collected and centrifuged at 80,000 *g* for 90 min. The collected precipitations were re-dispersed in phosphate buffer saline (PBS) solution and sonicated for 40 min to form cell membrane vesicles.

We used the Whatman polycarbonate membrane (Avantor, Radnor, PA, USA) to extrude the L-α-phosphatidylcholine (PC) vesicles [23]. Briefly, 5 mg of PC was dissolved in chloroform and dried under nitrogen for 2 h. After completely removing the chloroform, the PC was resuspended with PBS and sonicated for 20 min. The PC suspension was then extruded through a polycarbonate membrane (100 nm) to obtain PC vesicles. The prepared PC vesicles were stored at 4 °C for further use.

2.3. Preparation of cell membrane coated electrode

CMGS is fabricated by a top-down assembly process consisting of a gold electrode, enzyme hydrogel, and cell membranes. After aluminum oxide powder polishing, the gold electrode was activated by cyclic voltammetry scan in 0.5 M sulfuric acid and rinsed with water to remove impurities. Platinum nanoparticles (Pt NPs) were electrodeposited on the gold electrode at −2 V potential for 30 s (electroplating solution: 500 mM HCl, 5 mM chloroplatinic acid, and 5 mM lead acetate). 0.5 mL of polyvinyl alcohol (PVA) solution (4% (*m*/*m*)) was mixed with an equal volume of chitosan (CS) solution (2% (*m*/*m*)) and stirred for 30 min, followed by adding 10 μL of glycerol to increase the plasticity. 10 mg of glucose oxidase (GOx) was added into the PVA-CS mixture to form an enzyme-loaded hydrogel. 2.5 μL of enzyme-loaded hydrogel was dropped onto the Pt NPs electrode. 10 μL of cell membrane vesicles were dropped on the hydrogel coated electrode and dried at 35 °C for 15 min. The coating step was repeated three times to ensure that cell membranes completely covered the electrode surface. The PC vesicles were added on the cell membrane layer and dried at 50 °C for 30 min to promote the membrane integrity. The prepared CMGS was stored at room temperature and rinsed with water for three times to remove unfused vesicles.

2.4. CMGS electrochemical performance test

All CMGS tests were carried out under ambient temperature using a CHI-1000c electrochemical workstation with a three-electrode system. Ag/AgCl electrode (in saturated 3 M KCl solution) was used as the reference electrode, and a platinum wire was used as the counter electrode. I-t responses of the CMGS were recorded in 40 mL of PBS under 0.55 V potential with the addition of 2 mM glucose every 300 s. The error bar of each group was calculated based on three independently repeated experiments.

2.5. Measurement of glucose uptake in cultured cells

We measured the cellular glucose uptake process using glucose update assay kit. Tumor cells were seeded into 96-well plates and cultured overnight before being washed twice with PBS solution. 100 μL of Krebs-Ringer-Phosphate-Hepes buffer with 2% bovine serum albumin was added into each well and incubated for 40 min to keep the cells starved. Different GLUT1 inhibitors were added to co-culture with cells for 20 min to inhibit GLUT1 transport, followed by the addition of 10 mM 2-deoxyglucose (2-DG). After 20 min of incubation, the cells were lysed with extraction buffer. The extracted solution was mixed with the reaction kit and analyzed by a microplate reader in kinetic mode at 412 nm. The docking study of GLUT1 inhibitors and Western blot were described in the Supplementary data.

3. Results and discussion

3.1. Sensing concept and design

The CMGS used to screen GLUT1 inhibitors includes an Au-Pt NPs electrode, enzyme-hydrogel layer and cell membranes coated over the electrode (Scheme 1). Real-time monitoring of GLUT transport kinetics requires stable electrochemical sensors and functional membrane proteins in vitro. PVA-CS hydrogel layer served as a supportive layer for cell membrane fusion, while the loaded glucose oxidase (GOx) was employed for the electrochemical detection of transported glucose. GOx catalyzed the oxidation of transported glucose molecules into gluconic acid and hydrogen peroxide, which can be further catalyzed by Pt NPs on the Au electrode. We first optimized the concentration of GOx, and

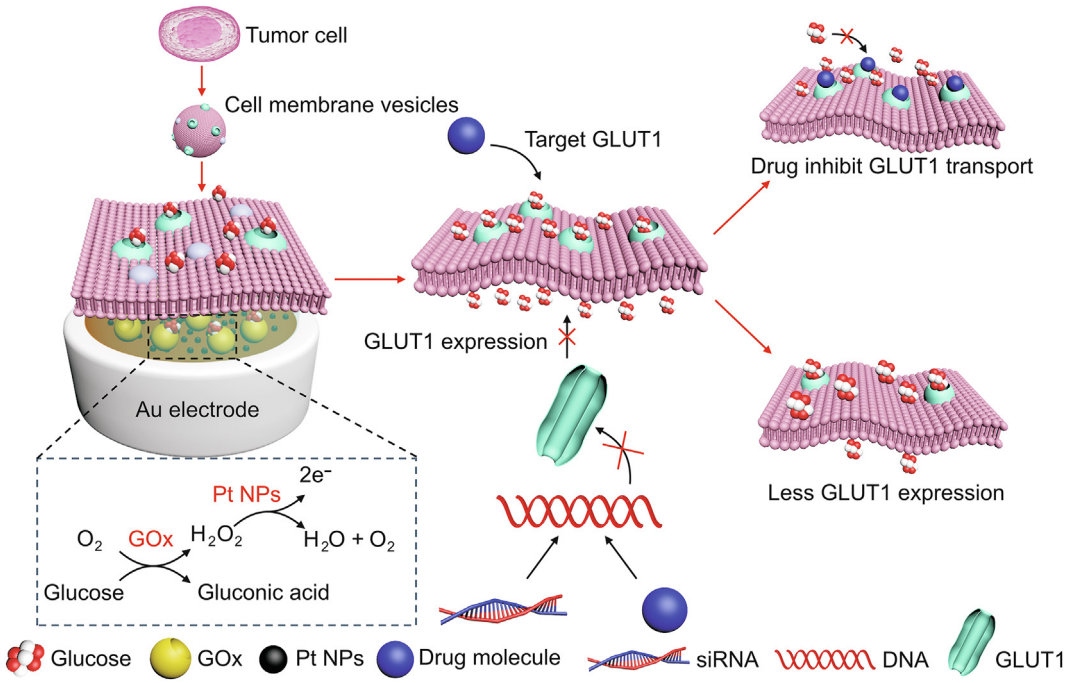

Scheme 1. Fabrication procedure and mechanism of the cell membrane-based glucose sensor (CMGS) for glucose transporter 1 (GLUT1) inhibitor screening. GOx: glucose oxidase; Pt NPs: platinum nanoparticles; siRNA: small interfering RNA.

determined that the GOx concentration in hydrogel with the highest sensitivity was 10 mg/mL (Fig. S1). In addition to the CMGS's sensing stability, the selective permeability of the cell membrane is another essential prerequisite for in vitro studies of transmembrane transport. The cell membrane fused with PC vesicles to form integrate and selectively permeable lipid bilayers. By combining a stable enzyme layer and a fused cell membrane, the CMGS provided an effective electrochemical platform for analyzing regulation of GLUT1 inhibition and expression.

3.2. Morphological characterization

The morphology and microstructure of the cell membrane coated electrode on CMGS were characterized by SEM and AFM. As shown in Fig. 1A, the surface of the enzyme-loaded hydrogel was smooth and flat, with root mean square (RMS) roughness under 100 nm (Fig. 1D), providing a bioaffinity layer for cell membrane fusion and maintaining in vitro bioactivity. Due to their complexity, cell membrane components could not spontaneously fuse to form a planar lipid bilayer on the hydrogel layer. When only cell membrane vesicles were coated (Fig. 1B), a porous surface with 15 μm diameters micropores and 1.2 μm RMS roughness were formed on the hydrogel (Fig. 1E), causing glucose rather than GLUT1 to reach the electrode via the micropores. Therefore, we added PC vesicles to facilitate cell membrane fusion and maintain the integrity of the planar lipid bilayer. As shown in Figs. 1C and F, after PC vesicles were added, the RMS roughness of the cell membrane electrode decreased to 500 nm without the appearance of obvious micropores, indicating that the cell membrane vesicles completely covered the surface of the hydrogel electrode.

3.3. Sensing performance of CMGS

Transmembrane proteins require the assistance of the lipid bilayer during the glucose transport process. In particular, the fluidity of the lipid bilayer maintained GLUT1 transport function in vitro [24]. We first used image-based FRAP to analyze the lateral mobility and fluidity of the fused cell membrane on the hydrogel layer. As shown in Fig. 2A, the quenched fluorescence on the membrane completely recovered within 700 s, indicating that the lipid bilayer maintained high fluidity for molecular diffusion on the hydrogel layer.

The integrity of cell membrane vesicles fused on the hydrogel surface was also critical for the in-vitro measurement of GLUT1 transport. We selected ascorbic acid (AA) as a signal molecule for integrity verification because it could be oxidized on an electrode under positive potential (Fig. S2) but could not be transported through an integral cell membrane. As shown in Fig. 2B, in the cell membrane coated sensor, the addition of 2 mM glucose resulted in a 110 nA current increase, whereas the addition of 250 μM AA only increased 5.3 nA, indicating that cell membrane vesicles fused into an intact planar lipid bilayer. The coated cell membrane, which ruptured and lost its transport capacity after 48 h, determined the working life of the CMGS, whereas the enzyme electrode retained its electrochemical activity for much longer than 48 h (Fig. S3). We also evaluated the selectivity of the CMGS for typical interfering molecules (Fig. 2C). The CMGS was tested in a solution of 2 mM glucose mixed with 100 μM uric acid or 250 μM AA. Compared with the current response which lacked interfering molecules, the relative current intensities of CMGS showed low variations of less than 4% (current response curve in Figs. S4). These results indicated that the CMGS had high selectivity and stability in the presence of the interfering molecules.

According to the Western blot results in Figs. 2D and S5, the expression of GLUT1 on tumor cell membranes (HepG2, MGC803, U87, A549, and H1299) was generally higher than that of normal cells (LO2 and RAW 264.7). To verify CMGS compatibility with different levels of GLUT1 expression, we coated electrodes with each of the aforementioned cell membranes. All coated sensors showed high linearity (R^2 > 0.99) in the glucose concentration range from 0 to 10 mM (Fig. S6), proving that the CMGS could couple with different cell membranes. As shown in Figs. 2E and F, electrodes coated with tumor cell membranes showed higher current response in addition of glucose. Specifically, after

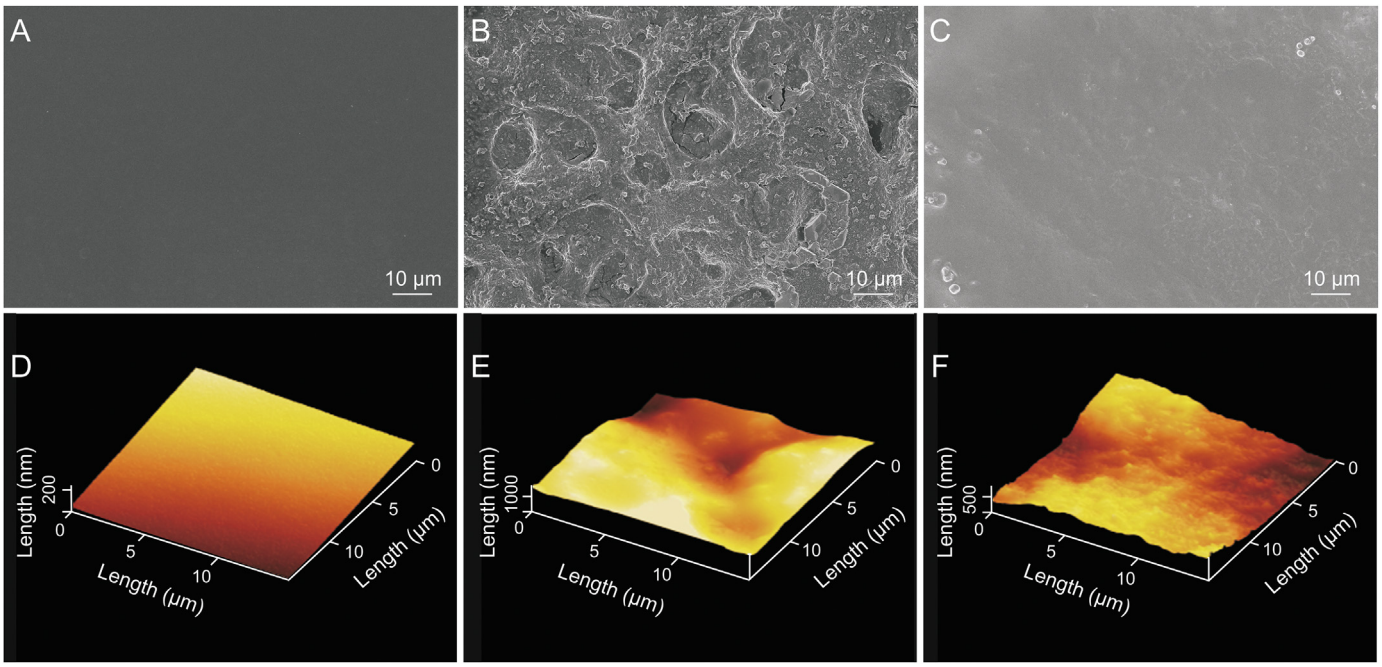

Fig. 1. (A–C) Scanning electron microscopy (SEM) and (D–F) atomic force microscopy (AFM) morphology of the cell membrane-based glucose sensor (CMGS). (A, D) The enzyme-loaded hydrogel layer. (B, E) Electrode surface coated only with cell membranes. (C, F) L-α-phosphatidylcholine (PC) vesicle-cell membrane coated electrode.

successive additions of 10 mM glucose, the amperometric response of LO2, RAW 264.7, H1299, HepG2, U87, MGC803, and A549 cell-originated CMGS increased 0.50, 0.67, 0.79, 0.78, 0.83, 0.86, and 1.07 μA, respectively. The higher current responses in the tumor cell group were consistent with the Western blot results, showing that CMGS could retain the glucose transport characteristics of various cell membranes.

3.4. CMGS compatibility with GLUT1 down-regulated membranes

After demonstrating the CMGS can couple with native cell membranes from different origins, we further investigated the performance of GLUT1 down-regulated cell membranes on CMGS (Fig. 3A). Interference molecules and siRNA could induce gene-specific down-regulation of GLUT1 expression localized on the

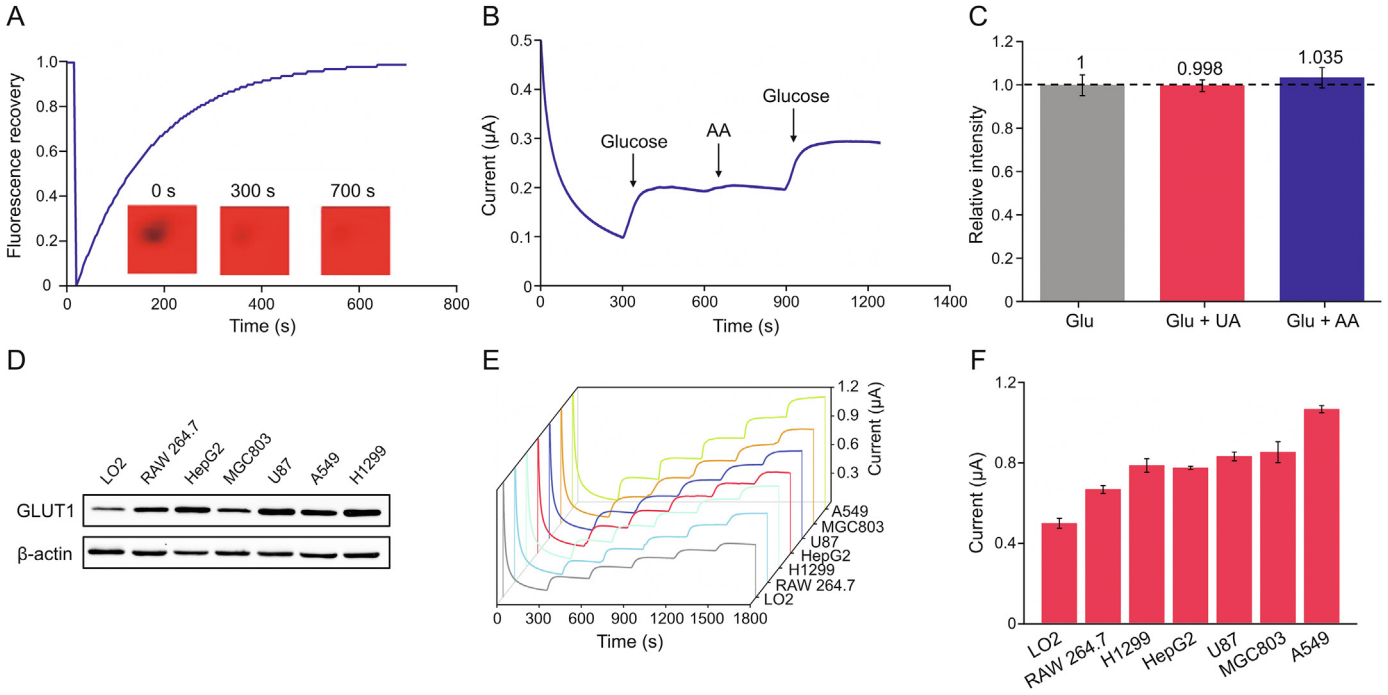

Fig. 2. Sensing performance of cell membrane-based glucose sensor (CMGS) to glucose. (A) Fluorescent recovery after photobleaching (FRAP) characterization of cell membrane coated on the electrode surface. (B) CMGS integrity verification by the addition of ascorbic acid (AA). (C) CMGS selectivity test ($n = 5$). (D) Western blot analysis of glucose transporter 1 (GLUT1) in different cell membranes. (E) Continuous current responses of CMGS coated with different cell membranes to 10 mM glucose. (F) Total current responses of CMGS coated with different cell membranes to 10 mM glucose.

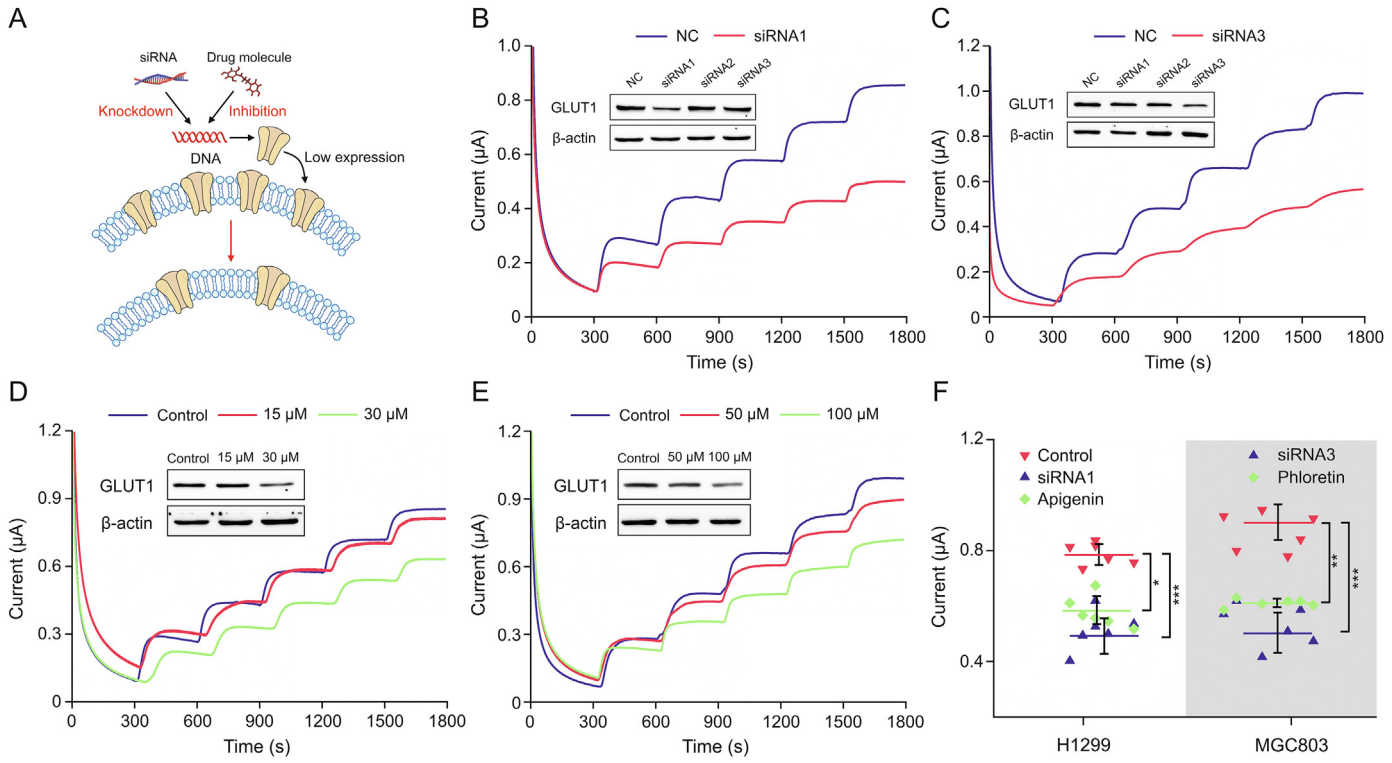

Fig. 3. Testing of compatibility between cell membrane-based glucose sensor (CMGS) and glucose transporter 1 (GLUT1) down-regulated membranes. (A) The mechanism of small interfering RNA (siRNA) and small drug molecules interfering GLUT1 expression. (B) siRNA1 knockdown GLUT1 expression (insert figure) in H1299 cells and current response of CMGS to glucose. (C) siRNA3 knockdown GLUT1 expression (insert figure) in MGC803 cells and current response of CMGS to glucose. (D) Apigenin down-regulated GLUT1 expression (insert figure) in H1299 cells and current response of CMGS to glucose. (E) Phloretin down-regulated GLUT1 expression (insert figure) in MGC803 cells and current response of CMGS to glucose. (F) Current difference between siRNA, drug molecules down-regulated group, and untreated group. $^{*}P < 0.05$; $^{**}P < 0.01$; and $^{***}P < 0.001$. NC: negative control.

cell membrane, leading to the decrease of glucose uptake in the targeted cells [25]. We designed and synthesized three siRNAs to transfect H1299 and MGC803 tumor cells to down-regulate the expression of GLUT1. According to the RT-qPCR results in Fig. S7, after 60 h of siRNA transfection, GLUT1 mRNA in H1299 cell decreased to 16.9%, 45.0%, and 8.5% of the negative control (NC) group, respectively. GLUT1 mRNA in the MGC803 cell decreased to 26.8%, 29.3%, and 14.6% of the NC group, respectively, indicating that siRNA was successfully transfected into the cells. As shown in the Western blot results (Figs. 3B and C), siRNA1 could effectively reduce GLUT1 expression in H1299 cells, while siRNA3 could reduce GLUT1 expression in MGC803 cells.

After validating the knockdown effect of siRNA, we coated the CMGS electrode with GLUT1 down-regulated $H1299_{siRNA1}$ and $MGC803_{siRNA3}$ cell membranes. The current response of $H1299_{siRNA1}$ CMGS to 10 mM glucose reached 0.50 μA, while that of the normal H1299 CMGS was increased 0.79 μA (Fig. 3B). With the same concentration of glucose, the current response of $MGC803_{siRNA3}$ CMGS reached 0.53 μA, while the normal MGC803 CMGS was increased 0.87 μA (Fig. 3C). The siRNA knockdown efficiency for GLUT1 was 72.1% and 67.7% in H1299 and MGC803 cells, respectively, while the current response of CMGS decreased to 62.5% and 60.9% in H1299 and MGC803 cells respectively, in the NC group. This indicated that test results for the CMGS were positively correlated with GLUT1 knockdown efficiency.

We further investigated the effect of GLUT1 regulation by small molecule drugs in TCM. To knockdown the GLUT1 expression, we utilized the small molecule drug apigenin, which inhibits the expression of GLUT1 by downregulating the PI3K/Akt pathway [26,27]. We treated H1299 cells with different concentrations of apigenin for 24 h prior to cell membrane extraction. In the 15 μM apigenin-treated group (Fig. 3D), the current response of the CMGS to 2 mM glucose was close to that of the untreated group (0.16 μA vs. 0.19 μA), whereas the current response of the 30 μM apigenin-treated group dropped to 0.13 μA, 32% lower than that of the untreated group. The current test result was consistent with the Western blot analysis (inserted Fig. 3D), showing that lower GLUT1 expression was associated with lower CMGS current.

Phloretin, a classic GLUT1 expression inhibitor [12,28], was used to downregulate GLUT1 in MGC803 cells. The current response of CMGS under 50 μM and 100 μM phloretin treatment increased 0.85 μA and 0.61 μA, respectively (Fig. 3E). The 100 μM phloretin-treated group (Fig. S8A) and untreated groups (0.93 μA) showed a significant difference ($P < 0.01$) in current response, indicating that phloretin could inhibit GLUT1 expression in MGC803 cells, which was consistent with our Western blot results (inserted in Fig. 3E). These results proved that apigenin and phloretin down-regulated GLUT1 expression in a dose-dependent manner, with apigenin taking longer to achieve the same inhibitory effect. According to the results of a cell counting kit-8 (CCK-8) assay (Figs. S8B and C), the half maximal inhibitory concentration (IC_{50}) values of apigenin and phloretin were 40.23 ± 2.55 μM and 76.86 ± 2.45 μM, respectively, demonstrating that the greater downregulatory efficiency of apigenin was associated with stronger inhibition of tumor cell proliferation. Results from different treatments demonstrated that CMGS current response could accurately reflect changes in GLUT1 expression induced by siRNA and drugs (Fig. 3F), while traditional methods required more time to analyze these pharmacological effects.

3.5. CMGS verified drug inhibition of GLUT1

The inward-open conformation of GLUT1 provides extracellular binding sites for glucose and inhibitors (Figs. 4A–C) [29]. There is a growing demand to identify new GLUT1 inhibitors for cancer starvation therapy. BAY-876 is the most active and selective GLUT1 inhibitor described in the literature [30]; therefore, we chose it as a model drug to verify the CMGS's ability to monitor GLUT1 kinetics. As shown in Fig. S9A, after the H1299 cell membrane was treated with 50 nM BAY-876, the CMGS current response to 10 mM glucose dropped to 0.11 μA. Compared with 0.79 μA for the control group, the difference between control and BAY-876 groups was statistically significant (Fig. S9B, $P < 0.001$). To better compare the GLUT1-inhibitory effect, we introduced the concept of response ratio and defined it as the ratio of currents before and after the glucose addition, which could effectively minimize the interference by the initial current difference. In Fig. 4D, the response ratio was 1.36 in 50 nM BAY-876 group, 75.8% lower than 5.61 of the NC group, indicating that BAY-876 could inhibit GLUT1 transport at a low concentration level.

After verification with a recognized GLUT1 inhibitor, we further expanded to investigate curcumin and baicalin for their inhabitation effect. Curcumin is a natural anti-tumor product in TCM that inhibits the GLUT1/MT1-MMP/MMP2 signaling pathway, thereby regulating tumor metabolic uptake as well as preventing tumor invasion and metastasis [31]. In our next experiment, we used 100 μM curcumin to treat the H1299 cell membranes. Current response of the CMGS to 10 mM glucose reached 0.71 μA (Fig. S9B), with a normalized response ratio of 5.65 (Fig. 4D). There was no significant difference between the 100 μM curcumin group and the untreated group (response ratio = 5.61), suggesting that curcumin could not directly inhibit GLUT1 transport. These results indicated that the CMGS could validate the inhibitory effect and clarify the mechanisms of metabolism-regulating drugs based on response ratio changes.

3.6. Analysis of GLUT1-inhibitory effect of Scutellaria baicalensis

Baicalin is the main active component of *Scutellaria baicalensis* with pharmacological effects such as antibacterial, anti-tumor, and anti-oxidation. Previous studies have suggested that baicalin can regulate glucose metabolism in tumor cells [32,33]. Therefore, we used the CMGS to investigate the inhibitory effect of baicalin on GLUT1 transport. The current response ratios of the CMGS were found to be 4.90, 3.02, and 1.69 when treated with baicalin at concentrations of 50 μM, 100 μM, and 200 μM, respectively

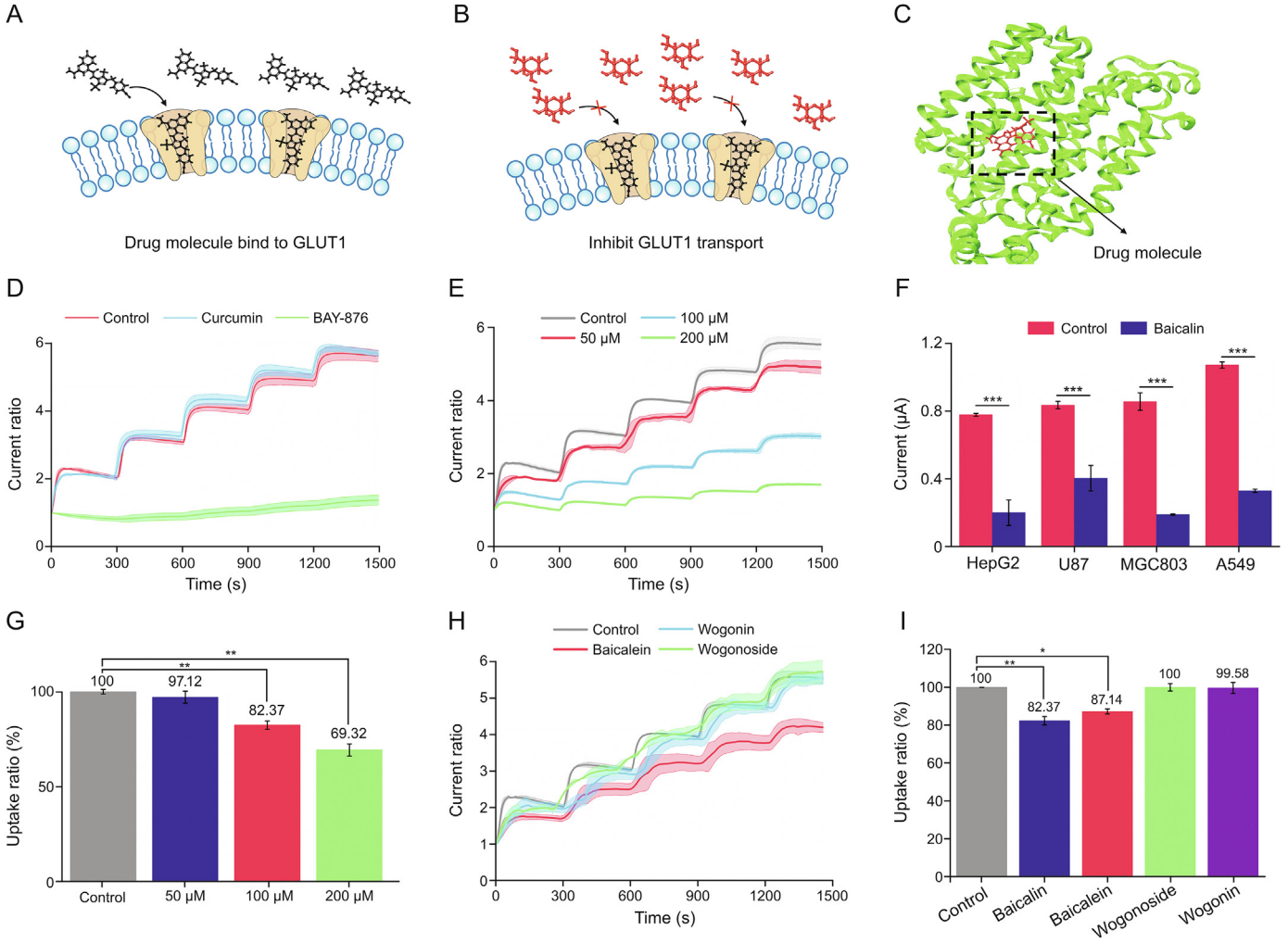

Fig. 4. Analysis of glucose transporter 1 (GLUT1)-inhibitory effect of small drug molecules. (A, B) The mechanism of small drug molecules inhibit GLUT1 transport and (C) molecular docking between drug molecules and GLUT1. (D) Current response ratios after BAY-876 and curcumin treatment. (E) Current response ratios of GLUT1 inhibited by different concentrations of baicalin. (F) Current responses of different cell membranes coated electrodes before and after baicalin inhibition. (G) The 2-deoxyglucose (2-DG) uptake ratios in H1299 cells treated with baicalin. (H) Current response ratios of baicalein, wogonin and wogonoside treated cell membrane-based glucose sensor (CMGS). (I) The 2-DG uptake ratios of H1299 cells treated with baicalin, baicalein, wogonin or wogonoside. $^{*}P < 0.05$; $^{**}P < 0.01$; and $^{***}P < 0.001$.

(Fig. 4E). Notably, these response ratios decreased by 87.3%, 53.8%, and 30.1% in a concentration-dependent manner compared with the untreated group (Fig. S10A, $P < 0.01$ for 100 μM group and $P < 0.001$ for 200 μM group). These results suggested that baicalin could inhibit GLUT1 transport with a concentration-dependent coefficient. CMGS tests on curcumin and baicalin demonstrated that the sensor could effectively detect drug inhibition of GLUT1.

We further tested the CMGS using four different kinds of tumor cells (HepG2, U87, MGC803, and A549) to verify the inhibitory effect of baicalin on GLUT1. After 200 μM baicalin treatment, the current response to 10 mM glucose increased 0.20, 0.40, 0.19, and 0.33 μA, respectively (Fig. 4F) and the current response curves of baicalin treated with different kinds of tumor cells were shown in Fig. S11. There were statistically significant differences from current response in untreated groups ($P < 0.001$), indicating that baicalin could inhibit GLUT1 transport in a variety of cell lines. In the cellular glucose uptake experiment, we utilized 2-DG, a non-metabolizable glucose analogue, to validate the results of the CMGS. In Figs. 4G and S10B, the 2-DG uptake ratio of 200 μM baicalin-treated H1299 cells dropped to 69.32% of that of the untreated group, a significant difference similar to that found for the CMGS ($P < 0.01$). Furthermore, a CCK-8 assay of cell viability (Fig. S10C) showed that the baicalin inhibited cell proliferation with a concentration-dependent coefficient. These results demonstrated that CMGS could accurately verify the GLUT1 inhibitory effect without depending on conventional cell assays.

Many bioactive compounds in *Scutellaria baicalensis* have chemical structures similar to that of baicalin (Fig. S12), including baicalein, wogonin, and wogonoside, all of which have a 2-phenylchroman skeleton, but their GLUT1 inhibiting effect remains unclear. We treated H1299 cell membranes with these bioactive compounds at a concentration of 100 μM. The current responses of CMGS treated with 100 μM baicalein, wogonin, and wogonoside increased 0.55, 0.63, and 0.61 μA (Figs. S13A–C), respectively, with normalized response ratios of 4.20, 5.49 and 5.65 (Fig. 4H). While the normalized response ratios of the wogonin and wogonoside groups were close to that of the untreated group, the baicalein-treated group showed a significant difference (Fig. S13D, $P < 0.05$), suggesting that baicalein might interfere with GLUT1 transport. In the 2-DG uptake test, the uptake ratios of H1299 cells treated with 100 μM baicalein, wogonin, or wogonoside were 87.14%, 99.58%, and 100% of the NC group, respectively (Figs. 4I and S13E), which was in line with our CMGS findings. We can conclude from the experimental results of both CMGS and 2-DG uptake that baicalein could inhibit cellular glucose uptake, but the inhibitory effect was weaker than baicalin [34]. In short, the CMGS enabled faster data acquisition than the cellular glucose uptake method.

We used molecular docking to verify CMGS and 2-DG uptake test results. The C domain of the GLUT1 channel provided the binding sites for small molecules and formed the hydrogen bond network with residues including ASN 317 from TM8, GLN 282, GLN 283 and ASN 288 from TM7, and ASN 415 from TM11.5 [34,35]. As depicted in Fig. S14, the binding of baicalin to GLUT1 involved seven hydrogen bonds, while the binding of baicalein, wogonin, and wogonoside to GLUT1 involved four, four, and three hydrogen bonds, respectively. The docking score showed that the order of binding strength with GLUT1 was as follows: baicalin > glucose ≈ baicalein > wogonon > wogonoside. The docking results were consistent with the CMGS test results, indicating that the CMGS test results were accurate and reliable.

3.7. CMGS screening for active components in catechins

Catechins are polyphenol compounds found in TCMs, tea, and berries with antioxidant activity. It has been reported that catechin compounds can inhibit the proliferation of tumor cells by regulating cellular glucose metabolism [36]. However, catechins are relatively unstable and easily oxidized to isoforms with similar structures, making it challenging to clarify the pharmacological mechanism. Therefore, we used the CMGS to determine catechin monomers's inhibitory effect on GLUT1. EGCG, the main monomer of catechins, was first investigated for its ability to inhibit the transport capacity of GLUT1 [37]. After the H1299 cell membrane was treated with 50, 100 and 200 μM EGCG, the normalized response ratios of the CMGS were 5.14, 3.64, and 2.17 (Figs. 5A and S15A), equivalent to 91.6%, 64.9%, and 38.7% of those of the untreated group, respectively. 100 μM and 200 μM EGCG groups showed significant differences from the untreated group (Fig. 5B, $P < 0.01$ for 100 μM and $P < 0.001$ for 200 μM). In the 2-DG uptake assay (Fig. 5B and S15B), the uptake rates of 100 μM and 200 μM EGCG-treated H1299 cells were 52.6% and 48.7% of those of the untreated group, demonstrating results consistent with those of the CMGS tests. Then we selected four different tumor cell membranes (HepG2, U87, MGC803, and A549) to expand the inhibitory target of EGCG. The current responses (Figs. 5C and S16) to 10 mM glucose in all four types of EGCG-treated cells were significantly lower than that of the untreated group ($P < 0.001$). According to CMGS test results on different cell membranes, EGCG had inhibitory effects on GLUT1 in tumor cells.

Catechins all have a 2-phenylbenzodihydropyrane structure (Fig. S17) but contain a variety of monomers owing to the isomerization of epi-type catechins during processing [38,39]. To investigate the pharmacological mechanism by which catechins regulated cellular metabolism, we employed the CMGS to determine the inhibitory effects of catechins derivatives. We used 200 μM concentrations of catechin derivatives, including catechin, epicatechin (EC), gallocatechin (GC), epigallocatechin (EGC), and epicatechin gallate (ECG) to treat the cell membrane. After treatment, CMGS current responses to 10 mM glucose were increased 0.63, 0.79, 0.55, 0.67 and 0.79 μA (Figs. 5E and S18A–E), corresponding to normalized response ratios of 5.49, 5.21, 4.62, 4.37 and 4.24 (Fig. 5D). We also used 2-DG uptake to verify the effects of these derivatives on cellular glucose uptake (Figs. 5E and S18F). Compared with the untreated group, the uptake ratios of EC, ECG, catechin, GC, and EGC were 92.2%, 84.0%, 88.8%, 87.8%, and 87.4%, respectively. Both CMGS and 2-DG test results showed no significant difference between catechin derivative groups and the untreated group, indicating that, unlike EGCG, other catechin derivatives could not inhibit cellular glucose uptake.

To better understand the inhibitory effect of catechins on glucose transport, we performed a unified cluster analysis of the current response and cell 2-DG uptake as measured in the experiment. As shown in Fig. 5F, the catechin, ECG, GC, EGC, and untreated groups were clustered together, while EGCG was clustered in isolation. According to the classification and summary of all data, cluster analysis results comprehensively reflected the inhibitory effect of catechins on GLUT1. We further constructed a three-dimensional model of experimental data using principal component analysis (PCA) in Fig. 5G. Compared with the results of cluster analysis, PCA results reflected data classification status more intuitively. The EGCG group was once again clustered separately, while the other monomers and untreated group were clustered together, indicating that EGCG had a better inhibitory effect on GLUT1. We also tested the effect of catechins on cell viability using the CCK-8 assay. The H1299 cell viability under 200 μM EGCG treatment for 24 h was 8.48%, while the cell viability of other catechins monomer groups exceeded 57.28% (Fig. 5H). As in the CMGS test results, EGCG exerted anti-tumor

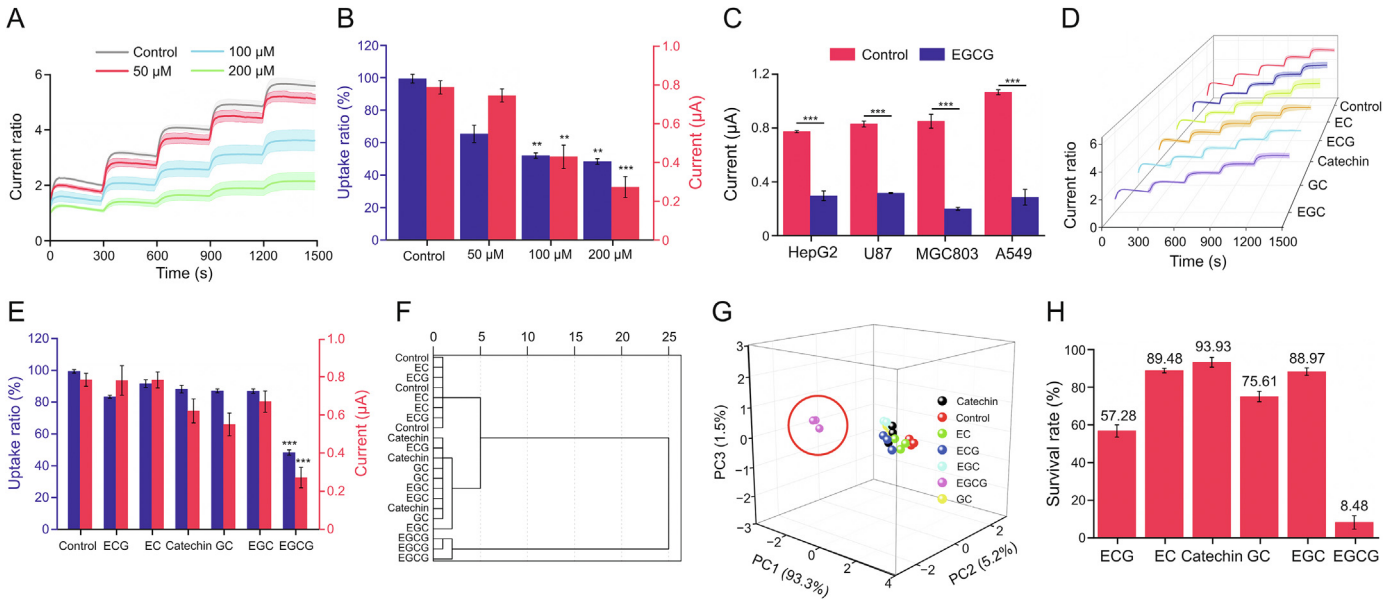

Fig. 5. Screening test of cell membrane-based glucose sensor (CMGS) towards active components in catechins. (A) Current response ratios of CMGS treated with different concentrations of epigallocatechin gallate (EGCG). (B) Current responses of CMGS and corresponding 2-deoxyglucose (2-DG) uptake ratios after EGCG treatment at different concentrations (blue histogram: the uptake rates of different concentration EGCG-treated H1299 cells; red histogram: the current response of CMGS treated with different concentration EGCG). (C) Current responses of CMGS coated with different cell membranes treated with EGCG. (D) Current response curves of CMGS treated with different catechin monomers. (E) Current responses of CMGS treated with catechin monomers and the corresponding 2-DG uptake ratios (blue histogram: the uptake rates of dcatechin monomers treated H1299 cells; red histogram: the current response of CMGS treated with catechin monomers). (F) Cluster analysis and (G) principal component analysis of CMGS current responses and 2-DG uptake ratios treated with catechin monomers. (H) The survival rate of H1299 cells treated with different catechin monomers. $^{**}P < 0.01$ and $^{***}P < 0.001$, compared with the control group. EC: epicatechin; ECG: epicatechin gallate; GC: gallocatechin; EGC: epigallocatechin.

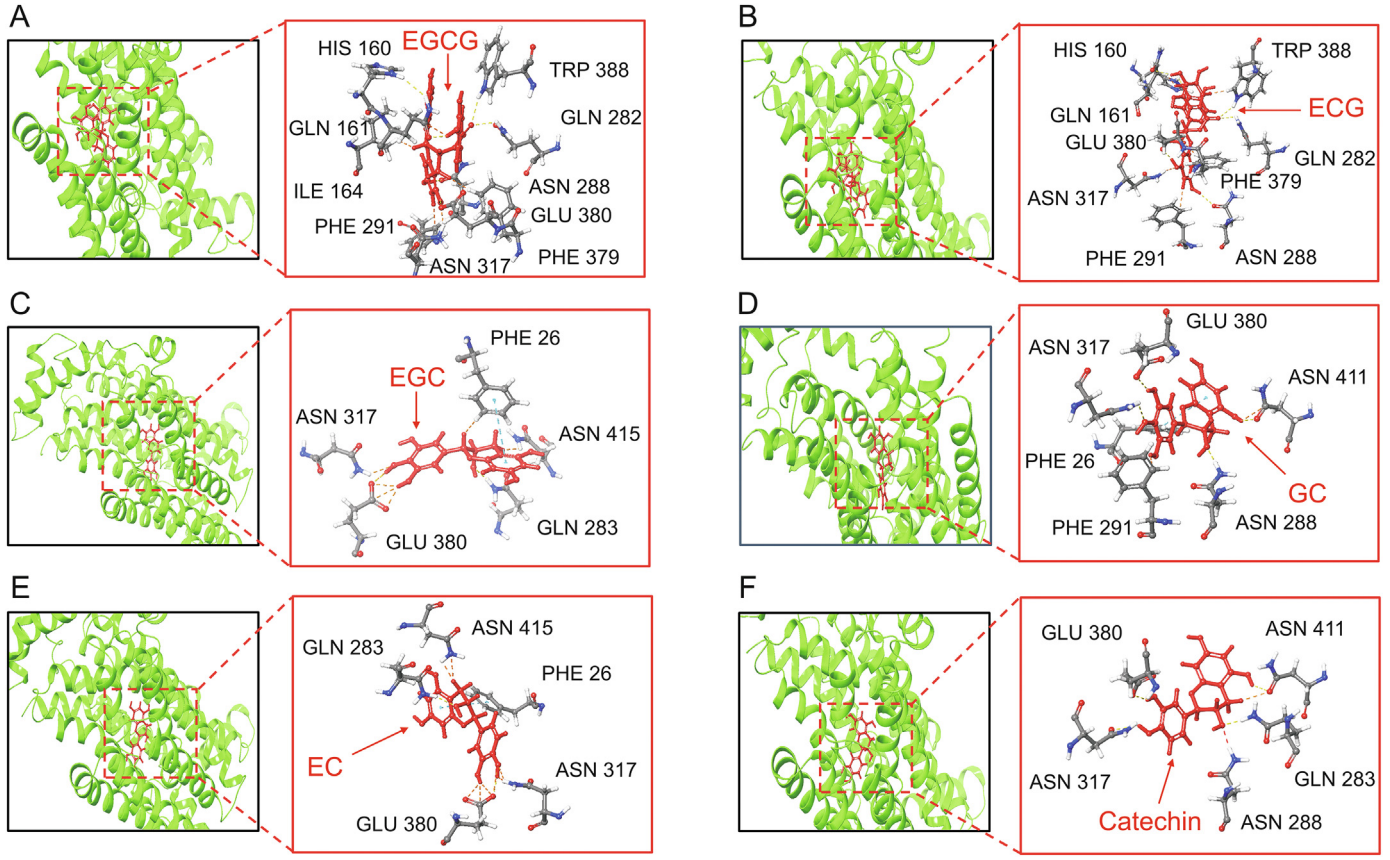

Fig. 6. Molecular docking and analysis of interactions between (A) epigallocatechin gallate (EGCG), (B) epicatechin gallate (ECG), (C) epigallocatechin (EGC), (D) gallocatechin (GC), (E) epicatechin (EC), (F) catechin, and glucose transporter 1 (GLUT1).

activity by interfering with the glucose uptake process of tumor cells. These results also demonstrated that CMGS could screen for effective components that inhibited GLUT1 transport from similar structures in catechins.

To validate CMGS test results on catechins, we also employed molecular docking in the experiment. As shown in Fig. 6A, EGCG-GLUT1 binding involved ten hydrogen bonds, whereas the glucose binding involved seven hydrogen bonds (Fig. S19), with TRP 388, GLN 282, and ASN 288 from EGCG-GLUT1 binding being the same as glucose-GLUT1 binding. The binding affinity of EGCG to the active site of GLUT1 was significantly higher than that of glucose, resulting in restricted glucose transport. The molecular structure of ECG is one hydroxyl less than that of EGCG (Fig. S17B), resulting in molecular configuration variation. There are nine hydrogen bonds in ECG-GLUT1 binding, weaker than the affinity of EGCG-GLUT1 (Fig. 6B), suggesting that variation in molecular configuration will affect the inhibitory effect. For other catechin derivatives docking results (Figs. 6C–F), the binding of EGC, GC, EC, and catechin to GLUT1 involved five, six, five, and five hydrogen bonds, respectively. GLN 283 and ASN 415 from EGC-GLUT1 binding, ASN 288 and ASN 411 from GC-GLUT1 binding, GLN 283 and ASN 415 from EC-GLUT1 binding, and ASN 288, GLN 283 and ASN 411 from catechin-GLUT1 binding were the same as glucose-GLUT1 binding. The binding to GLUT1 of these derivatives was weaker than that of EGCG but comparable to that of glucose. When these catechin derivatives are bound to GLUT1, glucose may compete for their binding sites, allowing the constant glucose transport process. This docking study revealed that the order of binding strength with GLUT1 was as follows: EGCG > ECG > EC > catechin > EGC > GC, which was consistent with CMGS test results. The molecular docking study demonstrated that CMGS could screen and identify the effective inhibiting monomer among similar molecule structures. Combining with other methods, CMGS has the potential to rapidly identify the pharmacological mechanism in the membrane protein domain as well as the ability to be used for derivatives screening.

4. Conclusion

In this study, we integrated tumor cell membranes on enzyme-loaded hydrogel electrodes to monitor GLUT1 transport kinetics and screen for inhibitors in TCM. The electrochemical response of the CMGS was found to be positively correlated with GLUT1 expression level and degree of inhibition. Our CMGS was compatible with a variety of cell membranes, including tumor cells and siRNA or drug-regulated cell membranes. This work demonstrated examples of GLUT1 inhibitor verification provided in this article, including BAY-876 and curcumin achieved via the analysis of CMGS current response. In short, we conclusively showed that the CMGS could accurately screen for potent GLUT1 inhibitors in *Scutellaria baicalensis* and catechins families, performing very similarly to the traditional cellular assay but more rapidly. Future demonstrations of this technology will focus on achieving kinetic monitoring of other membrane proteins and targeting receptor effects on the cell membranes.

CRediT author statement

Jiaqian Zhao: Methodology, Investigation, Formal analysis, Writing - Original draft preparation; **Yuqiao Liu:** Investigation, Data curation; **Ling Zhu:** Investigation; **Junmin Li:** Investigation; **Yanhui Liu:** Data curation; **Jiarui Luo:** Validation; **Tian Xie:** Project administration, Resources, Supervision; **Dajing Chen:** Conceptualization, Project administration, Writing - Reviewing and Editing, Resources.

Declaration of competing interest

The authors declare that there are no conflicts of interest.

Acknowledgments

This work was supported by the National Natural Science Foundation of China, China (Grant Nos.: 61801160 and 81730108).

Appendix A. Supplementary data

Supplementary data to this article can be found online at https://doi.org/10.1016/j.jpha.2023.04.015.

References

[1] K.J. Na, H. Choi, H.R. Oh, et al., Reciprocal change in glucose metabolism of cancer and immune cells mediated by different glucose transporters predicts immunotherapy response, Theranostics 10 (2020) 9579–9590.
[2] X. Jiang, J. Wu, M. Ke, et al., Engineered XylE as a tool for mechanistic investigation and ligand discovery of the glucose transporters GLUTs, Cell Discov. 5 (2019), 14.
[3] L. Sylow, M. Kleinert, E.A. Richter, et al., Exercise-stimulated glucose uptake-regulation and implications for glycaemic control, Nat. Rev. Endocrinol. 13 (2017) 133–148.
[4] T.M. Cheng, H.L. Chu, Y. Lee, et al., Quantitative analysis of glucose metabolic cleavage in glucose transporters overexpressed cancer cells by target-specific fluorescent gold nanoclusters, Anal. Chem. 90 (2018) 3974–3980.
[5] Y. Wang, J. Li, Z. Chen, et al., A GLUTs/GSH cascade targeting-responsive bioprobe for the detection of circulating tumor cells, Chem. Commun. (Camb) 58 (2022) 3945–3948.
[6] S. Wu, K. Zhang, Y. Liang, et al., Nano-enabled tumor systematic energy exhaustion via zinc (II) interference mediated glycolysis inhibition and specific GLUT1 depletion, Adv. Sci. (Weinh) 9 (2022), e2103534.
[7] A. Zaritski, H. Castillo-Ecija, M. Kumarasamy, et al., Selective accumulation of galactomannan amphiphilic nanomaterials in pediatric solid tumor xenografts correlates with GLUT1 gene expression, ACS Appl. Mater. Interfaces 11 (2019) 38483–38496.
[8] Y.-Y. Song, Y. Yuan, X. Shi, et al., Improved drug delivery and anti-tumor efficacy of combinatorial liposomal formulation of genistein and plumbagin by targeting Glut1 and Akt3 proteins in mice bearing prostate tumor, Colloids Surf. B Biointerfaces 190 (2020), 110966.
[9] W. Jiang, X. Luo, L. Wei, et al., The sustainability of energy conversion inhibition for tumor ferroptosis therapy and chemotherapy, Small 17 (2021), e2102695.
[10] A.R. Guerra, M.F. Duarte, I.F. Duarte, Targeting tumor metabolism with plant-derived natural products: Emerging trends in cancer therapy, J. Agric. Food Chem. 66 (2018) 10663–10685.
[11] J.W. Jang, H. Kim, I. Kim, et al., Surface functionalization of enzyme-coronated gold nanoparticles with an erythrocyte membrane for highly selective glucose assays, Anal. Chem. 94 (2022) 6473–6481.
[12] R. Singh, S. Kumar, F. Liu, et al., Etched multicore fiber sensor using copper oxide and gold nanoparticles decorated graphene oxide structure for cancer cells detection, Biosens. Bioelectron. 168 (2020), 112557.
[13] N. Wang, S. Zhang, Y. Yuan, et al., Molecular basis for inhibiting human glucose transporters by exofacial inhibitors, Nat. Commun. 13 (2022), 2632.
[14] F. Shao, Y. Wu, Z. Tian, et al., Biomimetic nanoreactor for targeted cancer starvation therapy and cascade amplificated chemotherapy, Biomaterials 274 (2021), 120869.
[15] J. Hong, M. Kang, M. Jung, et al., T-cell-derived nanovesicles for cancer immunotherapy, Adv. Mater. 33 (2021), e2101110.
[16] X. Liu, X. Gao, L. Yang, et al., Metal-organic framework-functionalized paper-based electrochemical biosensor for ultrasensitive exosome assay, Anal. Chem. 93 (2021) 11792–11799.
[17] J. Chang, H. Li, T. Hou, et al., Paper-based fluorescent sensor via aggregation induced emission fluorogen for facile and sensitive visual detection of hydrogen peroxide and glucose, Biosens. Bioelectron. 104 (2018) 152–157.
[18] C. Gu, X. Kong, X. Liu, et al., Enzymatic biofuel-cell-based self-powered biosensor integrated with DNA amplification strategy for ultrasensitive detection of single-nucleotide polymorphism, Anal. Chem. 91 (2019) 8697–8704.
[19] H. Wu, C. Shi, Q. Zhu, et al., Capillary-driven blood separation and *in situ* electrochemical detection based on 3D conductive gradient hollow fiber membrane, Biosens. Bioelectron. 171 (2021), 112722.
[20] I. Kim, D. Kwon, D. Lee, et al., A highly permselective electrochemical glucose sensor using red blood cell membrane, Biosens. Bioelectron. 102 (2018) 617–623.
[21] I. Kim, D. Kwon, D. Lee, et al., Permselective glucose sensing with GLUT1-rich cancer cell membranes, Biosens. Bioelectron. 135 (2019) 82–87.
[22] J. Zhao, C. Wang, X. Zhang, et al., Cell membrane coated electrochemical

sensor for kinetic measurements of GLUT transport, Anal. Chim. Acta 1226 (2022), 340263.
[23] Y. Luo, J. Zhao, X. Zhang, et al., Size controlled fabrication of enzyme encapsulated amorphous calcium phosphate nanoparticle and its intracellular biosensing application, Colloids Surf. B Biointerfaces 201 (2021), 111638.
[24] S.H. Huang, B-C. Huang, L. Chao, Development of cell membrane electrophoresis to measure the diffusivity of a native transmembrane protein, Anal. Chem. 94 (2022) 4531–4537.
[25] L. Li, L. Li, W. Li, et al., TAp73-induced phosphofructokinase-1 transcription promotes the Warburg effect and enhances cell proliferation, Nat. Commun. 9 (2018), 4683.
[26] Y.M. Lee, G. Lee, T.I. Oh, et al., Inhibition of glutamine utilization sensitizes lung cancer cells to apigenin-induced apoptosis resulting from metabolic and oxidative stress, Int. J. Oncol. 48 (2016) 399–408.
[27] X. Chen, J. Tan, L. Zhang, et al., Apigenin ameliorates vascular injury in rats with high fructose-induced metabolic disturbance by inhibiting PI3K/AKT/GLUT1, RSC Adv. 8 (2018) 24470–24476.
[28] S.Y. Lee, J-H. Park, S-H. Ko, et al., Mussel-inspired hyaluronic acid derivative nanostructures for improved tumor targeting and penetration, ACS Appl. Mater. Interfaces 9 (2017) 22308–22320.
[29] P.M. Ung, W. Song, L. Cheng, et al., Inhibitor discovery for the human GLUT1 from homology modeling and virtual screening, ACS Chem. Biol. 11 (2016) 1908–1916.
[30] R. Commander, C. Wei, A. Sharma, et al., Subpopulation targeting of pyruvate dehydrogenase and GLUT1 decouples metabolic heterogeneity during collective cancer cell invasion, Nat. Commun. 11 (2020), 1533.
[31] J. Liu, C. Zhang, R. Wu, et al., RRAD inhibits the Warburg effect through negative regulation of the NF-κB signaling, Oncotarget 6 (2015) 14982–14992.
[32] N. Kong, X. Chen, J. Feng, et al., Baicalin induces ferroptosis in bladder cancer cells by downregulating FTH1, Acta Pharm. Sin. B 11 (2021) 4045–4054.
[33] P. Fang, M. Yu, L. Zhang, et al., Baicalin against obesity and insulin resistance through activation of AKT/AS160/GLUT4 pathway, Mol. Cell. Endocrinol. 448 (2017) 77–86.
[34] R. Wu, K. Zhu, X. Zhang, et al., Nonimmobilized biomaterial capillary electrophoresis for screening drugs targeting human glucose transporter 1, Anal. Chem. 89 (2017) 12951–12959.
[35] D. Deng, C. Xu, P. Sun, et al., Crystal structure of the human glucose transporter GLUT1, Nature 510 (2014) 121–125.
[36] O.A. Ojelabi, K.P. Lloyd, J.K. De Zutter, et al., Red wine and green tea flavonoids are *cis*-allosteric activators and competitive inhibitors of glucose transporter 1 (GLUT1)-mediated sugar uptake, J. Biol. Chem. 293 (2018) 19823–19834.
[37] J.J. Gu, K.S. Qiao, P. Sun, et al., Study of EGCG induced apoptosis in lung cancer cells by inhibiting PI3K/Akt signaling pathway, Eur. Rev. Med. Pharmacol. Sci. 22 (2018) 4557–4563.
[38] Q. Wu, B. Zhao, G. Sui, et al., Phytochemicals block glucose utilization and lipid synthesis to counteract metabolic reprogramming in cancer cells, Appl. Sci. 11 (2021), 1259.
[39] I. Peluso, M. Serafini, Antioxidants from black and green tea: From dietary modulation of oxidative stress to pharmacological mechanisms, Br. J. Pharmacol. 174 (2017) 1195–1208.